Journal of Advanced Joining Processes 13 (2026) 100391

Contents lists available at ScienceDirect

Journal of Advanced Joining Processes

journal homepage: www.sciencedirect.com/journal/journal-of-advanced-joining-processes

Numerical analysis of the robustness of self-pierce riveting with pre-formed joining partners

J.-P. Ludwig *, E. Tolke, M.C. Schlichter, M. Bobbert, G. Meschut

Laboratory for Material and Joining Technology (LWF), Paderborn University, Paderborn, Pohlweg 47-49, 33098, Germany

ARTICLE INFO

Keywords:
Self-pierce riveting
FE modelling
Plastic pre-deformation
Meta modelling

ABSTRACT

Modern industrial development has necessitated a wide range of joining technologies. Self-pierce riveting has become a prevalent technique for sheet metal assembly, especially in automotive applications. Achieving proper joint geometry and adequate load-bearing capacity depends on appropriate tool selection and precise process control. Material properties and condition also play a significant role in process performance. To accommodate the inevitable variations in component characteristics during production, a robust and stable joining process is essential. The study focuses on investigating the influence of preformed joining partners on the joining process and the joint's load capacity. An EN AW-6014 in T4 condition, as well as an HCT590X, are used as materials for this study. For this purpose, an exemplary process chain consisting of the steps of performing, joining, and shear load testing is studied. Each process step is implemented using an FE model to predict the outcome of subsequent steps. For analysis of the influence of pre-strain, an optimisation software is used to plan and execute variations of the process. These variations are used to create a meta-model that can describe the relationships between pre-forming and characteristic parameters of subsequent process steps. The resulting model is validated by comparing simulation and experimental data. Finally, in a novel approach, the robustness of the presented process chain is analyzed in terms of a tolerable performance level for the joining partners.

Introduction

Driven by regulatory standards and rising consumer demands, the automotive sector faces pressure to reduce greenhouse gas emissions through new vehicle designs. A highly effective approach to meeting these environmental objectives involves implementing multi-material assemblies, which enable optimized material use and maximize potential weight savings (Meschut et al., 2014). Consequently, the ongoing pursuit of lightweight materials and novel manufacturing techniques creates significant challenges for connection technologies. Self-pierce riveting represents an effective joining method for connecting dissimilar sheet materials. The self-pierce riveting (SPR) process can be described as follows. The joining partners are joined using a semi-tubular rivet, as shown in Fig. 1. Two metal sheets are generally used as joining partners. These sheets are placed between a punch and a die. In the first step, a blank holder holds the sheets between the punch and die sides without plastic deformation of the joining partners. Afterwards, the punch drives the self-piercing rivet through the punch-sided sheet. Pressing the rivet towards the die causes the die-sided sheet to expand in the die. The increased resistance of the expanded material, as well as certain die geometries, promotes the spreading of the rivet foot, creating an interlock of the SPR and thus a form lock in the joint. For this joining operation, no pre-punched hole is necessary. In addition, the joint is media-tight at least from the die side, as the rivet does not pierce the die-sided sheet in correctly joined parts. An extensive overview of the process and mechanical performance is given by Li et al. (Li et al., 2017).

The quality of SPR joints is assessed by measuring the extension of the interlock (f), the minimum remaining die-side material thickness (t_r), and the rivet head position (P_h) (Meschut et al., 2014; Neuser). These characteristic geometric values can be determined through measurements on the cross-section of a joint's micrograph. For different combinations of material composition and sheet geometry (MGC) of the joining partners, various SPR geometries and tools are required to produce joints of adequate quality. Optimisation of joint properties is a current area of research. Zhao et al. investigated the joint-formation mechanisms for SPR, dependent on sheet thickness and rivet length and concluded that these variables had significant influence on the

* Corresponding author.
E-mail address: jean.patrick.ludwig@lwf.upb.de (J.-P. Ludwig).

https://doi.org/10.1016/j.jajp.2026.100391

Available online 10 March 2026

interlock formation (Zhao et al., 2022). In a 2022 study, the influence of rivet and die parameters on joint quality in SPR was investigated (Wang et al., 2022). The research team used a smooth particle Galerkin (SPG) algorithm to model the top sheet and thus solving the problem of material failure. Similar research was carried out by Karathanasopoulos et al. without the use of SPG particle algorithm (Karathanasopoulos et al., 2021). They successfully derived discrete values for die depth and rivet leg thickness for the investigated material combinations. Further research was done on the influence of tip geometry in SPR aluminium joints (Li et al., 2013). While no influence on fatigue strength could be determined, sharper rivet tips showed an increased lap shear strength. Xie et al. found that the sheet thickness ratio significantly affected the failure mode of lap-shear-tested SPR joints in cold-formed thin-walled steel structures (Xie et al., 2018). In a more recent investigation by Wang et al., the influence of heat treatment on the joint characteristics of steel-aluminium parts is researched (Wang et al., 2023). It is shown that energy absorption can be improved by heat treatment, whereas peak force is only slightly affected. Du et al. have shown the influence of rivet design on load-bearing capacity under quasi-static and dynamic loads and found similar mechanical responses of SPR joints to process parameters in both load cases (Du et al., 2021).

Throughout the life cycle of SPR-joined parts, various steps in the process chain influence joint characteristics. An entire life cycle includes the construction and manufacturing of the joining partners, the joining process, the service phase of the joint, and the recycling of the part. In this context, the load-bearing capacity is analyzed as a metric for the mechanical robustness of the joint during the service phase. This study focuses on the influence of the manufacturing process on joint quality and load-bearing capacity. Precisely, a pre-rolling process is performed on sheet materials, inducing stresses and strains. Rolling is a continuous or stepwise pressure forming process between parallel rollers that rotate in opposite directions. The resulting compressive stresses cause the material to flow plastically, compressing it in the thickness direction between the rollers and stretching it in the rolling direction (Primer on Flat Rollin, 2014). In cold-rolling without spreading, plane strain conditions apply, i.e., one of the main deformation rates is zero during the forming process. The available forming force is applied directly to the forming zone or rolling gap. Cold rolling can lead to work hardening and anisotropy. To determine the load-bearing capacity, shear load tests are conducted on the joints.

The influence of plastic pre-deformation on mechanical joints has been investigated in various studies. Bielak et al. have analysed the influence of pre-strain on characteristic geometric values in clinch joints under applied strains up to 0.6. By utilizing validated numerical models for straining and joining, a sensitivity analysis revealed the influence of preforming on the joinability of the investigated materials (Bielak et al., 2021). In a subsequent study, the process chain was expanded to include a shear lap tensile test (Bielak et al., 2021). Furthermore, the influence of anisotropy on clinch joints is shown to be minimal (Friedlein et al., 2023). In a recent review of the state of mechanical joint modelling, the authors conclude that these processes are well understood, while noting issues with depicting deformation-based damage. Current methods for describing joinability rely on trial-and-error (Meschut et al., 2022).

For SPR joints, it is shown for aluminium and steel, respectively, that pre-deformation of the joining sheets has a greater influence on the joint's characteristic geometrical values than on its load-bearing capacity (Hahn and Kurzok, 1998; Hahn and Kurzok, 1998). In a study by Han et al., an increase in pre-strain up to 3 % led to a higher shear strength in SPR-joined aluminium specimens (Han et al., 2006). The authors attributed this to work-hardening effects during pre-straining. Ma et al. derived a mathematical relationship between lap shear strength, top sheet thickness, and interlock (Ma et al., 2018). A simulation model incorporating sheet metal materials with pre-deformations up to 190 % was applied by Xue et al. to accurately represent the failure behavior of SPR joints under different loading scenarios (Xue et al., 2023). The simulations demonstrated accurate prediction of failure behavior for pre-deformed SPR joints under lap shear conditions. However, damage initiation and failure preceding the SPR joining of pre-deformed specimens remained unconsidered. In a 2024 study, Wang et al. investigated the joinability of SPR joints across various sheet stack combinations, focusing on optimised rivet geometries to improve joinability (Wang et al., 2024). In a recent study, the influence of rolling-induced sheet metal deformation on SPR joints was investigated (Schlichter et al., 2025). With the rise of artificial intelligence (A.I.), interest in resource-efficient predictive models is growing. Zhao et al. trained artificial neural networks (ANN) for prediction of key joint quality indicators in the joints' cross-section (Zhao et al., 2021).

This study focuses on the influence of pre-rolled joining partners on the geometrical characteristics and load-bearing capacity of SPR joints, with effective plastic strain (ε_p) up to 0.4, for multi-material and pure combinations. The study gains its novelty by the combination of the following key elements: (1) The systematic use of optimisation software coupled with meta-modelling to map the relationships between preforming parameters, joint characteristics and load-bearing capacity. (2) The determination of critical thresholds for tolerable performance levels to assess process robustness.

Material characterization and experimental details

This study was subject to various boundary conditions to investigate joint properties across the entire process chain. The materials used and the experimental details are explained below. The numerical model properties and process boundary conditions are described in the methodology section.

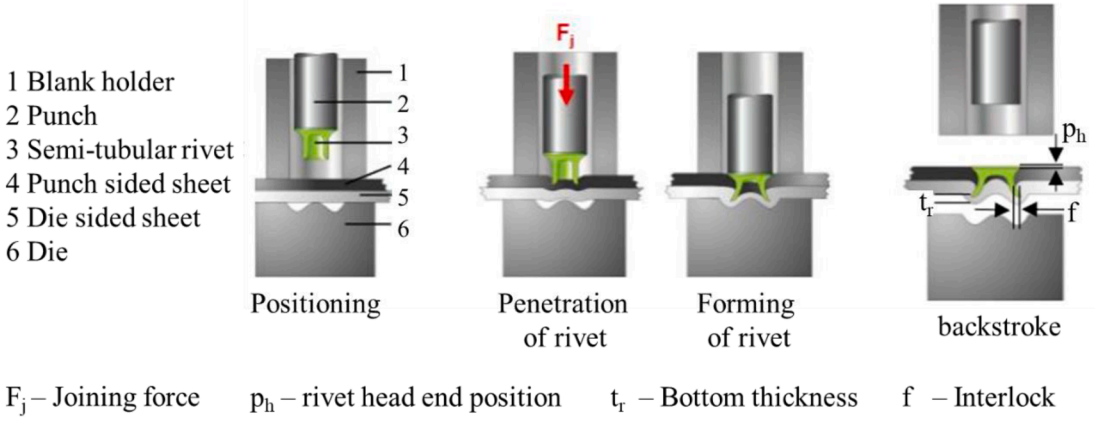

Fig. 1. Joining process for SPR based on (Meschut et al., 2014; Neuser).

For the experimental investigations of this study, a dual-phase steel HCT590X with a sheet thickness of 1.5 mm, a minimum yield strength of 330 MPa, and a minimum elongation at break of 20 % was used (Flachstahl, 2022). The microstructure consists of ductile ferrite phases with strengthening martensite inclusions in between. Because of its high tensile strength and strong work hardening properties, HCT590X is commonly used in automotive applications. An exemplary chemical composition can be seen in Table 1.

In addition, aluminium alloy EN AW-6014 T4 with a sheet thickness of 2.0 mm, a yield strength of 130 MPa, and a minimum elongation at break of 23 % was used (Novelis Global Automotive, 2019). An overview of chemical composition is given in Table 2.

The self-piercing rivets are manufactured from 38B2 alloy by cold-forming and subsequent tempering to H4 condition. The cemical composition as provided by the manufacturer is seen in Table 3. The material was heated to 855 °C-865 °C and subsequently quenched, following the manufacturer's recommendations. Further details for hardening of SPR made from 38B2 are provided in the work of Holtkamp et al. (2025). In accordance to H4 condition standards, the rivets reached 480 HV (Vickers hardness).

The mechanical properties of the used materials as provided by the suppliers are listed in Table 4. The values provided for 38B2 are given for the unhardened material condition.

Through experimental testing, flow curves were developed for use in the numerical modelling. These flow curves are shown in Fig. 2. The experimental data was taken from previous studies by (Böhnke et al., 2021). Common extrapolation approaches (Voce, Hocket-Sherby) were applied to extend the experimental data to cover the high strain levels occurring during the joining process.

The experimental results used to validate the numerical models presented in this study are from (Schlichter et al., 2025). For transparency, the different machines used in the experimental approach are presented in the following section.

Pre-rolling of sheet metal parts was performed using a Bühler & Co. rolling mill operated by the Institute of Manufacturing Technology (LFT) at Friedrich-Alexander-Universität Erlangen-Nürnberg (FAU), which enabled the production of pre-rolled specimens. The rolling mill features two electric motors capable of generating a maximum rolling force of 1.2 MN. The adjustable rolling gap ranges from 0 to 25 mm, while the rolls measure 210 mm in diameter with a barrel length of 300 mm.

The SPR joining process was carried out by the Laboratory for Material and Joining Technology (LWF) at Paderborn University on a TUCKER® TRT080 system with a servo-electric drive and a C-frame. All joining operations were carried out with a joining speed of 20 mm/s and a blank holder force of 2.15 kN. The die type was a FM095 2115, and the rivet type C 5.3 × 5.5 H4 was used throughout every material and thickness combination.

Shear tensile testing was performed on a Zwick Z100 tensile-compression testing machine at a strain rate of 10 mm/min. Specimens' geometries were based on the DVS 3480–1 specifications (Europäische Forschungsgesellschaft für Blechverarbeitung e.V, 2021).

Methodology and procedures

To determine the influence of prior process steps on later parts of the process chain, a numerical approach is utilized. Since this study concentrates on the process chain: pre-rolling of the joining partners (1), the SPR joining process (2), and the load-bearing capacity of the joints (3), a numerical model for each step is created. The results of each process are saved in LS-DYNA dynain files, including mesh geometry, effective plastic strain, and element-wise stress states. This enables further use in subsequent process steps and in the analysis of, e.g., the characteristic geometrical values of the SPR. The numerical approach enables a profound analysis of changes in the mechanical properties of the joint as well as allowing for an efficient way of calculating a high number of model variants to draw conclusions about joint robustness. The approach is shown in Fig. 3. In the first step, a Design of Experiments (DoE) is created by varying the degree of sheet thickness reduction for both joining partners during the rolling process. To enable a robustness analysis of the process chain, a minimum of 100 data points per MGC is planned, using the space-filling method in LS-OPT. After test planning, the process steps for each selected point are numerically simulated consecutively. The rollers for the rolling process are placed according to the selected data point to reduce the respective sheet to the desired thickness. Afterwards, the sheets are added to the joining process simulation. The result of this process is analysed with respect to geometrical values. In parallel, the 2D model is mapped to a 3D model for lap-shear tensile testing. The measured effective plastic strain from the rolling process, the geometric values of the joints' cross-sections, and the maximum shear load from the lap shear test are added to the meta-model database. After the complete DoE is completed, the data points are used for meta-modelling and the analysis of correlations among the aforementioned characteristic values.

For every numerical modelling of the process chain, LS-DYNA is used to describe the mechanical process. Explicitly, the solver smp_d_R910 is utilized. For model preparation between process steps, the LS-PREPOST version v4.12.4 is used. The Design of Experiments (DoE) for generating sample points was planned and executed in LS-OPT v7.0.0. In addition, Python scripts were used to evaluate joint characteristics and generate the meta-models shown in the results chapter.

For each numerical model, the same material model was used. Specifically, MAT_224 – Tabulated Johnson Cook was used, since elasto-viscoplastic material properties are adequately implemented using the flow curves mentioned previously. In addition, all models are solved with an implicit approach. This ensures stable convergence for the quasi-static problems presented in this study.

Table 1
Exemplary chemical composition for HCT590X (Flachstahl, 2022).

HCT 590X	C	Si	Mn	P	Al	Cr+Mo	Nb+Ti	V
min. mass- %	-	-	-	-	-	-	-	-
max. mass- %	0.15	0.75	2.50	0.04	1.5	1.40	0.15	0.20

Table 2
Exemplary chemical composition for EN AW-6014 T4 (Novelis Global Automotive, 2019).

EN AW-6014	Fe	Si	Mn	Cr	V	Ti	Cu	Mg
min. mass- %	-	0.30	0.05	-	0.05	-	-	0.40
max. mass- %	0.35	0.60	0.20	0.20	0.20	0.10	0.25	0.80

Table 3
Exemplary chemical composition for 38B2 (Werkstoff-Datenblatt).

38B2	C	Si	Mn	P	S	Cr	Cu	B
min. mass- %	0.35	0.15	0.60	-	-	-	-	0.0008
max. mass- %	0.40	0.30	0.90	0.025	0.025	0.30	0.25	0.0050

Table 4
Mechanical properties of the used materials (Flachstahl, 2022; Novelis Global Automotive, 2019; Werkstoff-Datenblatt).

Mechanical properties	Yield strength (MPa)	Ultimate strength (MPa)	Elongation at break(%)
HCT590X	330 – 430	590 – 700	$\geq$ 20
EN AW-6014 T4	$\leq$ 130	$\geq$ 175	$\geq$ 25
38B2	-	$\leq$ 660	$\geq$ 57

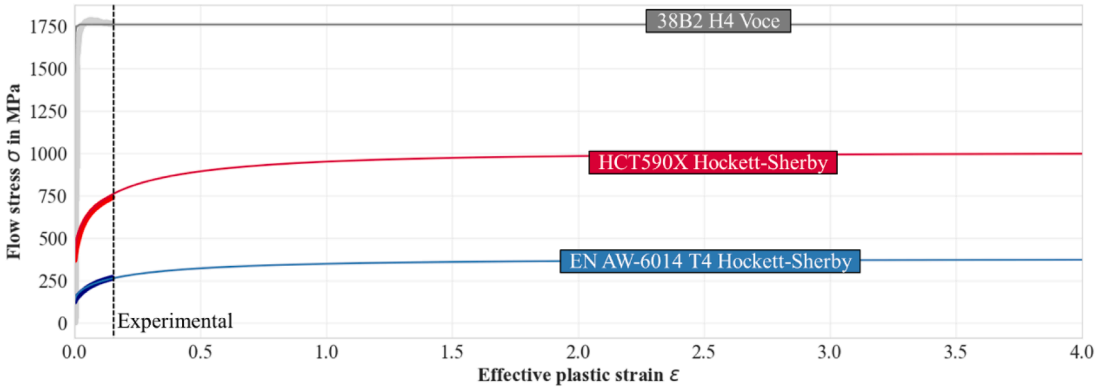

Fig. 2. Flow curves for materials.

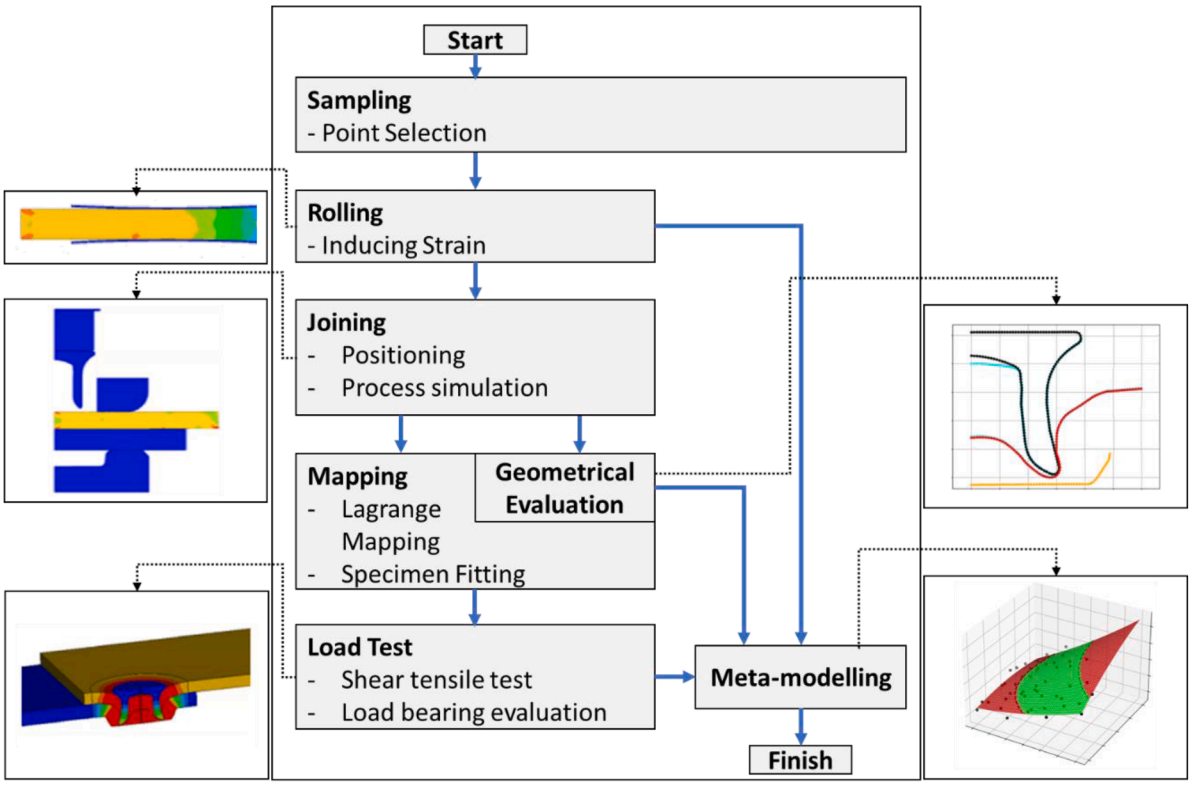

Fig. 3. Numerical method for the investigation of pre-forming on the quality of SPR joints.

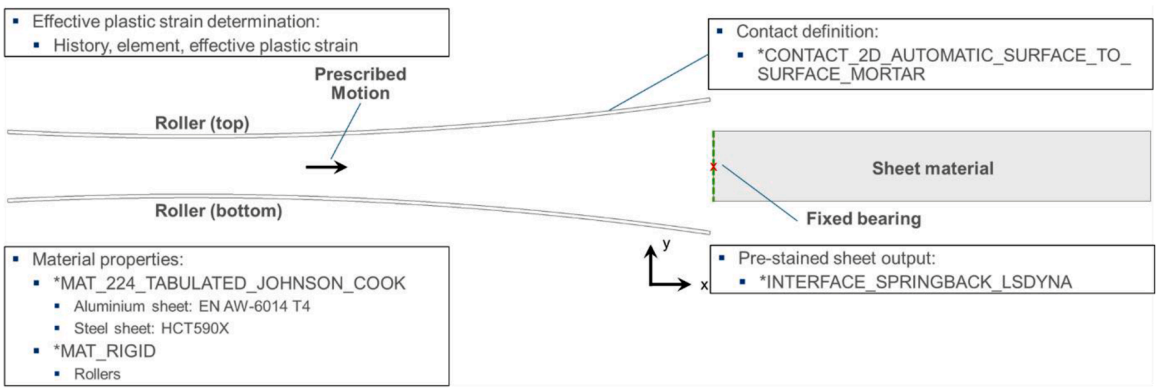

Fig. 4. Numerical model for rolling.

Rolling model

In preparation for the joining process, a rolling model was implemented. Fig. 4 shows the model and the important keywords used for modelling. Since the SPR process is simulated in 2D, the rolling process also uses shell elements of type 13. Two curved parts act as rollers. The to-be-rolled part is fixed at the side facing the rollers by using BOUNDARY_SPC_SET, stopping movement in both axes. Both rollers are modelled with a MAT_RIGID material model. To emulate the rolling process, the rollers are set to move along the rolled material until a sheet thickness reduction of up to 30 % is achieved. The results are saved in a dynain-file for usage in following process steps, including information of mesh geometry, effective plastic strain and stress states. Anisotropic behaviour is not considered by the material model, based on the study results of (Friedlein et al., 2023). The effect of material anisotropy introduced by the rolling process on the joint was investigated exemplarily for steel-steel connections as a supplementary study. The steel sheets were reduced by 30 % of the original sheet thickness to 1.1 mm and subsequently joined. The joining result was evaluated based on the geometric characteristics interlock and remaining bottom thickness, and both sides of the cross-section were compared. The differences were in the range of up to 0.02 mm, thus corresponding to the expected fluctuations caused by process and analysis variations. The rolling simulation serves primarily as a tool to generate the required sheet thickness reductions and pre-strains for our joining analysis. For this purpose, frictionless contact conditions were applied during rolling.

The sheets are then prepared for the joining simulation. To avoid duplicates, unique IDs are given to nodes, elements, and parts. In the LS-OPT procedure, this is done by calling command files (c-files) in LS-PREPOST. In addition, the effective plastic strain (EPS) resulting from the rolling procedure is tracked for further analysis. Additionally, the sheets are loaded into the joining simulation and positioned using another c-file.

Self-pierce riveting model

The SPR model is based on the works of Harabati et al. and adapted for this study (Harabati et al., 2025). An overview of the model and important keywords is given in Fig. 5. The parts are also meshed with element type 13 and an element length of 0.1 mm. The punch is moved by a constant motion towards the die. The blank holder is connected to the punch via a spring element, increasing the blank holder force continuously as the punch moves. The tools (punch, blank holder, and die) are modelled as rigid elements. The rivet is modelled with *MAT_024, which allows plasticity during joining. Movement is tracked by a history node chosen from the punch-mesh. Because of the high deformations in the sheets, an adaptive remesh is implemented using *CONTROL_ADAPTIVE. The process force is tracked by a cross-section in the die. For the contacts between both sheets and the sheets and the tools, a combined friction model is applied, and friction parameters are adjusted for model validation. The final coefficients are listed in Table 5. After successful termination, the joined sheets and rivet are saved in a dynain-file for further analysis and transfer to the shear tensile testing model.

The reduction in sheet thickness is also considered in the joining process. Fig. 6 shows the mathematical approach for this adaptation, which considers the punch distance, the original sheet thickness, and the reduction of both sheets. In addition, a small offset t of 0.007 mm is chosen to prevent overlap and numerical instability in the model. The positioning of the parts is implemented using the formula in *PARAMETER_EXPRESSION and *PART_MOVE.

To accurately depict the mechanical behaviour of SPR-joints under uniaxial shear load, the joining result must be mapped onto a 3D model of the specimen. This is done using a multi-step procedure, beginning

Table 5
Static friction coefficients for the SPR joining process contacts.

Contact	EN AW-6014 – EN AW-6014	HCT590X – EN AW-6014	HCT590X – HCT590X
Punch – rivet	0.20	0.20	0.20
Rivet – top sheet	0.20	0.23	0.21
Rivet –bottom sheet	0.20	0.23	0.23
Top sheet – bottom sheet	0.23	0.07	0.12
Bottom sheet - die	0.12	0.22	0.14

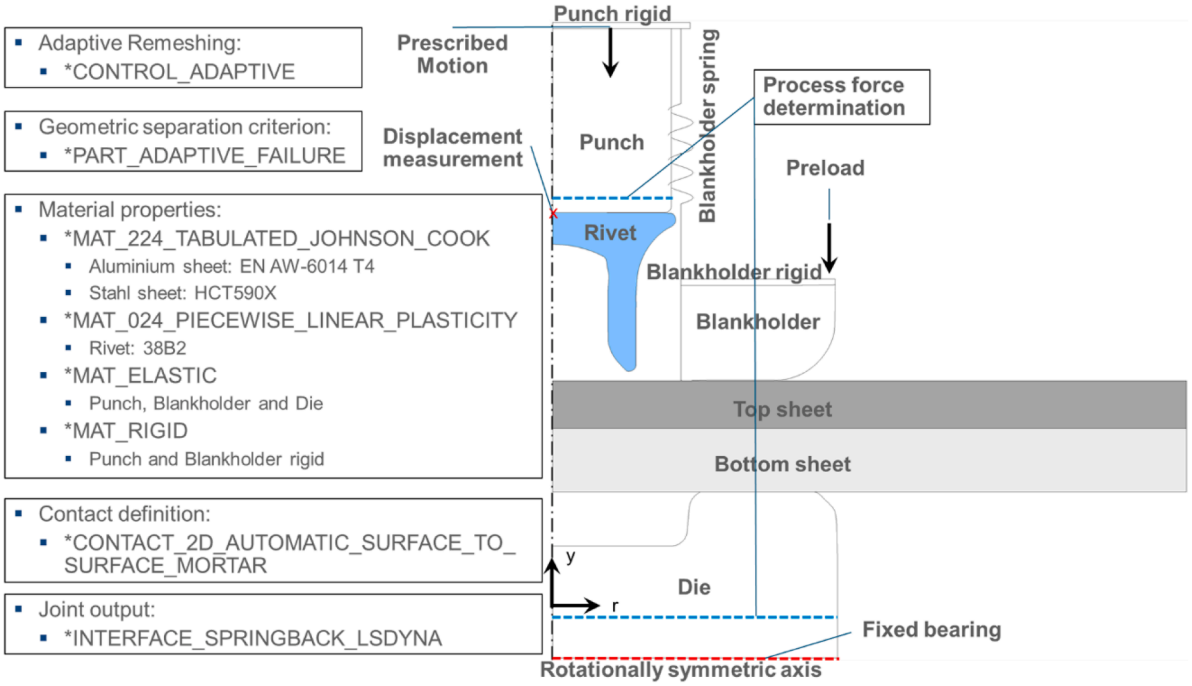

Fig. 5. Numerical model for the SPR joining process.

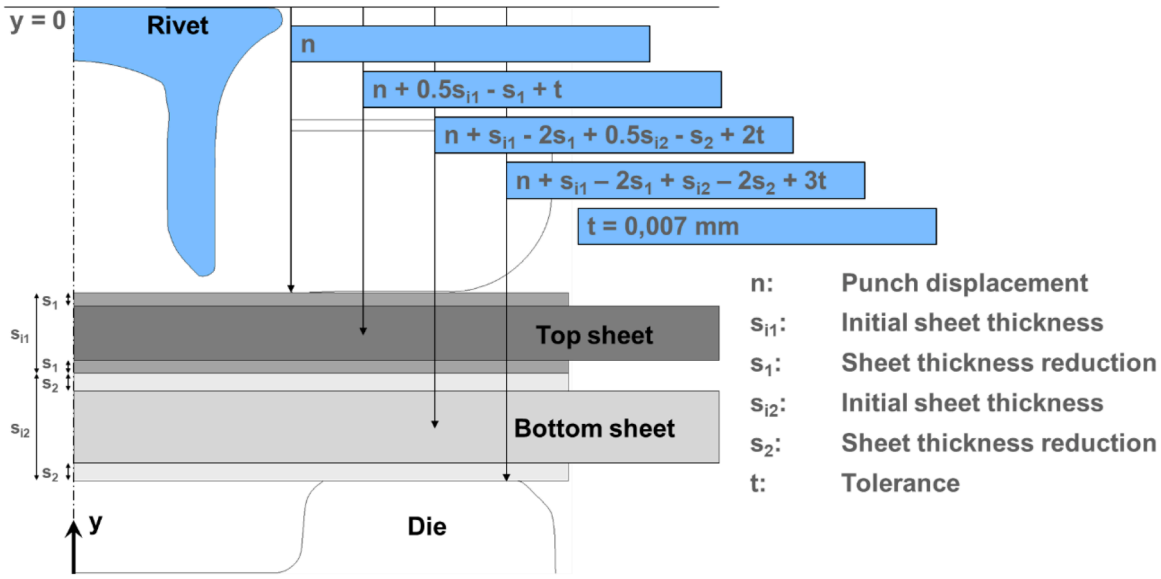

Fig. 6. Positioning of the sheets for SPR joining.

with trimming the joint to a radius consistent across the entire DoE. The radius is chosen to be as small as possible to increase simulation efficiency, but large enough to maintain the complete joint. Afterwards, the joint is remeshed.

The 2D shell mesh is then mapped to 3D solid elements using a Lagrangian Mapping algorithm. At first, *INITIAL_LAG_MAPPING_WRITE is used to create a map file for the relevant parts. In a second step, the parts are converted to a 3D mesh using 'INITIAL_LAG_MAPPING. The conversion is centred on the joint and rotated by 180 ° around the joint's vertical symmetry axis, creating a semi-model of the joint. As a cleanup step, prismatic elements generated by the mapping algorithm are deleted to avoid instabilities. The result is then exported to a dynain-file for use in the numerical model for tensile testing.

At the same time, the characteristic geometric values of the SPR joint are automatically measured using a Python script. The script takes measurements from the 2D-model and saves interlock and remaining bottom thickness for further analysis.

Shear tensile model

To accurately depict shear-tensile tests, the joint is embedded into a standardised specimen for shear-tensile testing. The model is shown in Fig. 7. The joint is connected to larger sheets for both joining partners using *CONTACT_TIED_NODES_TO_SURFACE_CONSTRAINED_OFFSET. These larger sheets are meshed with a larger element size to increase efficiency during the solving stage. Furthermore, the effective plastic strain in the joint's border areas is mapped to the larger sheets to account for work hardening. The shear-tensile test is done by locking the lower sheet's end against all degrees of freedom, while a constant motion is used to apply the load onto the specimen. The process force is again tracked by a cross-sectional plane, and the local displacements of the specimen are tracked by history nodes.

Results and discussion

The procedure described in the former chapter was applied as

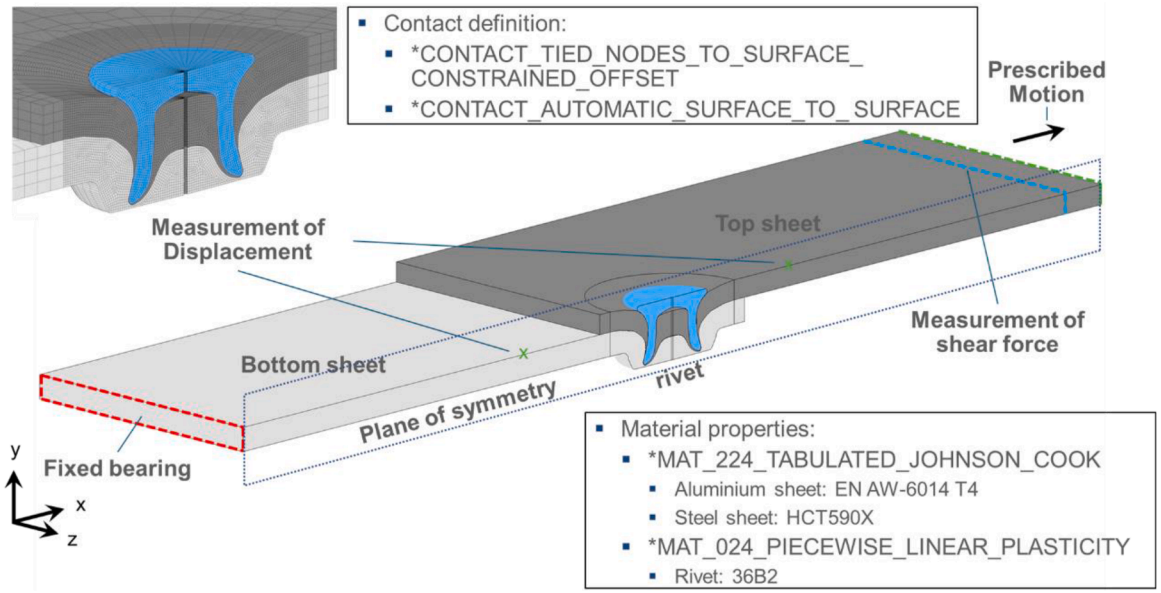

Fig. 7. Numerical model for shear testing.

explained, and the results are presented in the following order: First, the model validation is described and shown in detail for all material-thickness combinations. Afterwards, the results of the DoE are represented and discussed. The chapter ends with a summary of inferential conclusions regarding the correlations between process parameters and target values.

Model validation

The model of the preliminary rolling process served primarily to introduce pre-strains and sheet thickness reductions. Nevertheless, the modelling was validated through multiple steps. First, the sheet thickness reduction observed in the experiment was compared with that predicted by the simulation. The agreement was within ±0.01 mm, as shown in the contour lines in Fig. 8 and Fig. 9. Additionally, Vickers hardness tests were conducted. These averaged 239 HV1 for a forming strain of 0.3, which correlates with a tensile strength of approximately 770 MPa and corresponds to the flow stress of the material at this forming strain, as can be observed in Fig. 2.

The results of model validation for the joining process are presented in Fig. 8 and Fig. 9. In these figures, the contour lines of the numerical process results are layered above the cross-sectional view of the experimental specimen. Below the contour comparison, the measurements for characteristic geometric values are listed and compared for the simulation and the experiment. In Fig. 8, the results for sheets without prior thickness reduction and thus with an effective plastic strain of zero are presented. For St-Al and Al-Al MGC, good agreement is reached for the contour lines, the interlock, the bottom thickness, and the rivet head end position. The geometrical values for the Al-Al combination show greater deviations than those for the other combinations. The reduced spread of the rivet indicates that the model slightly underestimates the strength of the aluminium alloy. However, the experiment also shows greater deviations across all samples. Nonetheless, good agreement is reached for the contour lines. A similar assessment was achieved for the force-displacement graphs for the process across all combinations. The maximum force and the general shape of the graphs are also in good agreement.

The results for an effective plastic strain of 0.3 are shown in Fig. 9. For these results, generally good agreement is observed between the simulation and the experiment for the geometrical values and the contour lines. It is apparent that the remaining bottom thickness is slightly underestimated for all combinations, while the interlock is slightly overestimated for Al-Al and St-Al. When accounting for the scatter bands in the experimental data, the simulation still provides a sufficiently accurate approximation for investigating the influence of pre-forming. The force-displacement diagram for all combinations shows generally good agreement with the experiment, albeit the maximum force is slightly underestimated. The peaks in Fig. 8 for the St-St combination between a displacement of 3 to 4 mm occur after the rivets' penetration of the punch-sided sheet. The newly formed contact surfaces of the severed sheet metal and slug rub against the rivet shank. Simultaneously, the rivet experiences reduced resistance at the location of sheet metal separation and undergoes slight upsetting upon contact with the die-side sheet. During this process, all joining partners are remeshed multiple times, resulting in fluctuating force values. This behavior also explains the fluctuations in the process curves in Fig. 9 between 2 and 4 mm. Overall, the validation results indicate that the joining model is suitable for investigating the qualitative influence of pre-forming on the joint.

In Fig. 10, the maximum force from shear-tensile testing simulations is compared with the experimental results for all combinations with EPS set to 0 and 0.3. While the numerical model underestimates the forces, the comparison shows similar levels overall. The underestimation is most pronounced for the Al-Al combination, with more exact results for St-Al and Al-Al. The deviation in maximum shear load capacity could be

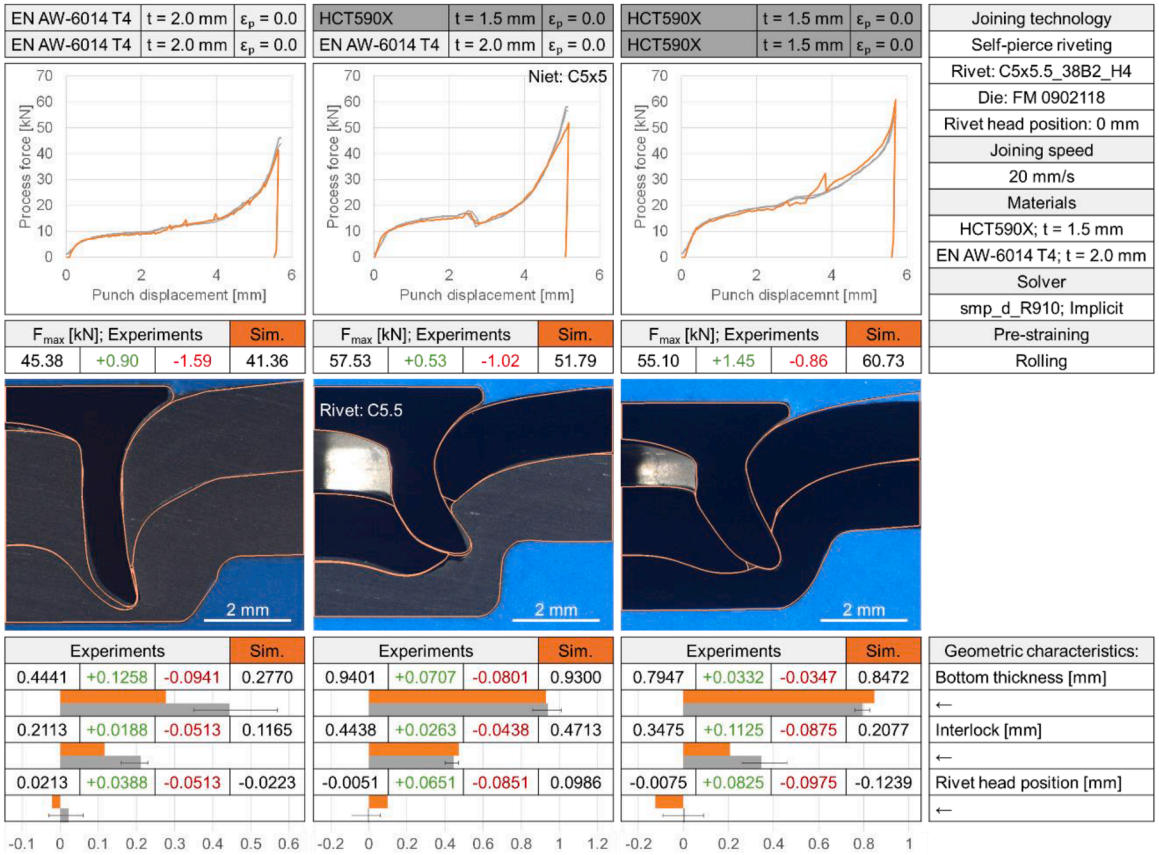

Fig. 8. Model validation of the SPR process for EPS = 0.

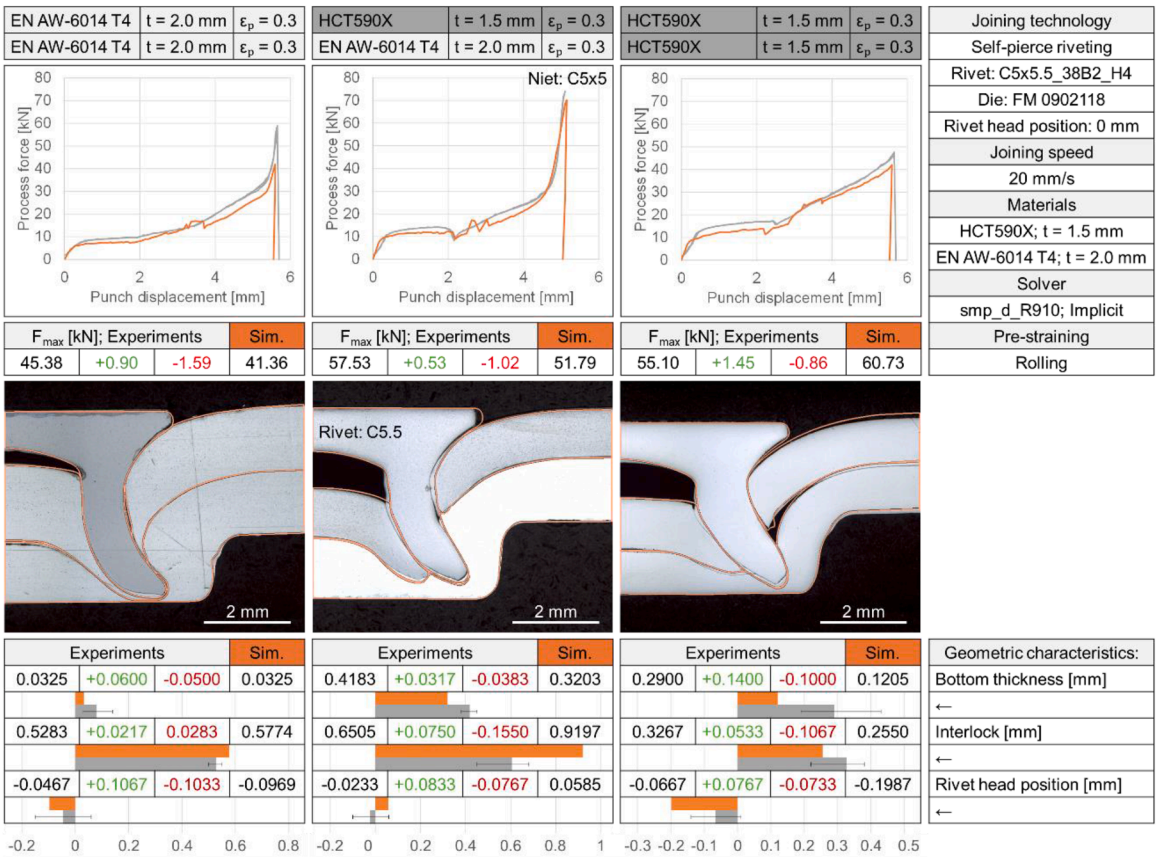

Fig. 9. Model validation of the SPR process for EPS = 0.3.

Fig. 10. Model validation of the shear load process simulation.

explained by the omission of a damage model during the process chain. Accumulating damage, especially for higher pre-strains introduced during rolling, could lead to different results seen in the experiment.

Model accuracy

For each MGC, a DoE was conducted with 100 data points at the minimum sample size. Pre-forming was carried out to an EPS of 0.4, after which the numerical model became increasingly unstable, with the rivet piercing the bottom sheet and contacting the die. Given the approximately linear correlation between sheet thickness reduction and equivalent plastic strain (EPS), the maximum sheet thickness reduction was limited to 40 %. For the originally 2 mm thick aluminum sheet, this corresponds to a maximum reduction to 1.2 mm, and for the 1.5 mm steel sheet, a reduction to 0.9 mm. The forming process parameters and the output variables of the joining and lap shear tensile testing process were incorporated into the meta-modelling approach. Fig. 11 illustrates the output variables interlock and remaining bottom thickness, as well as the maximum lap shear force, as a function of the sheet metal forming strain. Response surface models (RSM) were employed to identify trends within the data clouds. These are represented in green and red in the figure. Values in the green areas are within specification for the respective measurement, whereas red areas indicate out-of-specification values. The specification is based on industrial standards. The models were developed with a quadratic polynomial regression model. To evaluate RSM accuracy, the R^2 Value was calculated.

Most models showed R^2 values above 70 %, indicating correlations between the analysed target values. The process chain for the Al-Al combination showed greater instability with increasing EPS of the upper sheet, thereby reducing the available data points for RSM extrapolation. The model must be evaluated with caution. For example, the Al-Al model for maximum shear force shows a strong decline in the top sheet's EPS after an initial increase. This behaviour is based on a relatively small sample size of EPS above 0.15 for both sheets, as reflected in the relatively low R^2-value. However, the available data points above 0.15 support the general shape of the RSM. The remaining bottom thicknesses for the Al-Al and St-St combinations fall below the critical limit values at an effective plastic strain level above a certain threshold for both sheets. For Al-Al, this limit is reached earlier than for the St-St combination. The St-Al combination reaches the critical threshold for the bottom thickness across all data points. In addition, the RSM for the interlock shows low accuracy with a R^2 of 0.60. The quadratic approach used for RSM still showed the highest R^2 value. This indicates that no trend is detectable for mixed-material combinations, even though every data point was within specifications.

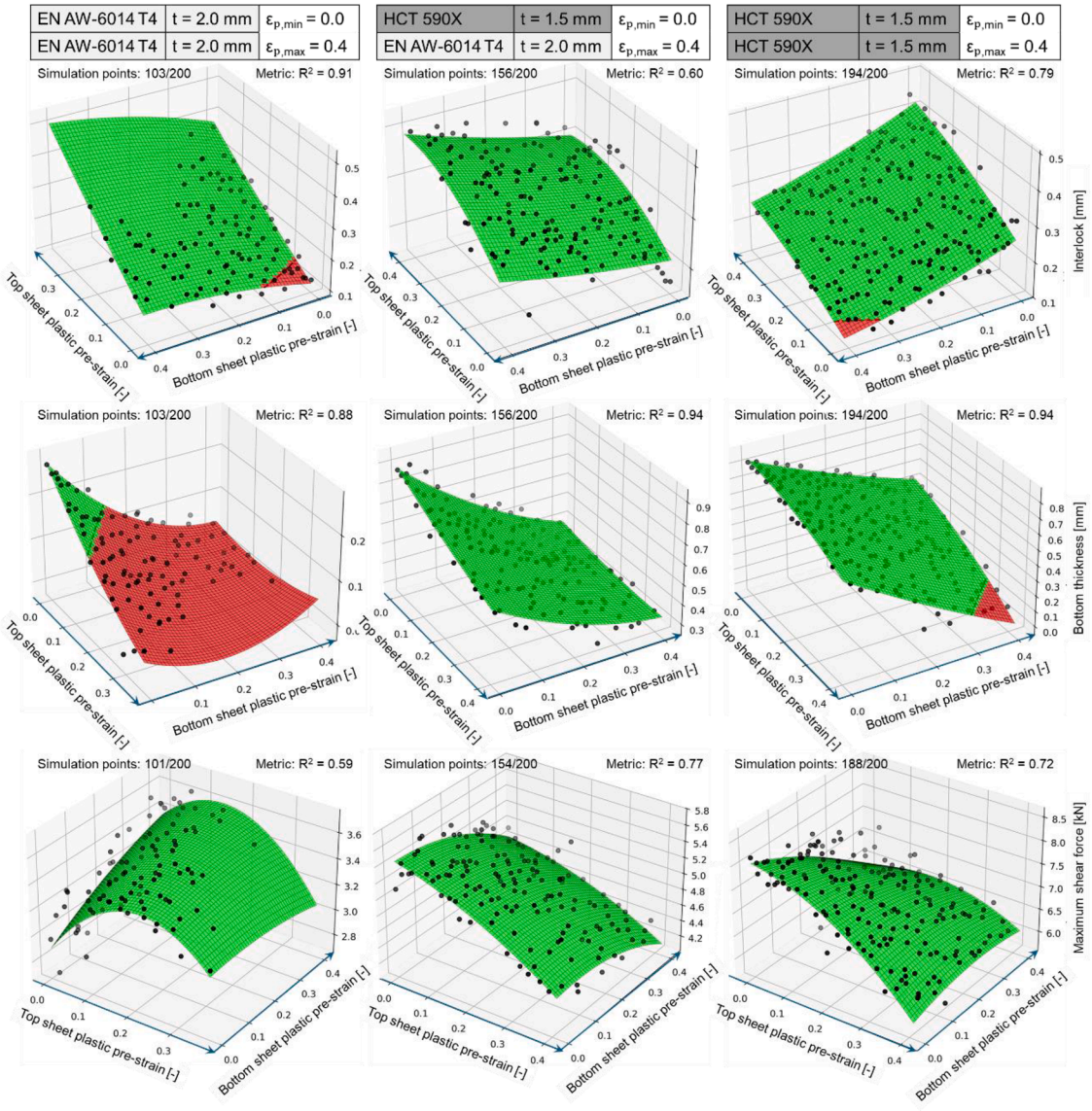

Fig. 11. Pre-strain influence on various output variables along the process chain.

Effects on target features

From the RSM in Fig. 11, certain qualitative statements can be derived regarding the correlations among effective plastic strains, the interlock, the remaining bottom sheet thickness, and the maximum shear force.

Depending on the material-thickness combination, the effect on the joint quality and load-bearing capacity varies. Higher plastic strains in the top sheet of the Al-Al combination lead to an increase in interlock, whereas this effect is observed to a smaller margin for the bottom sheet pre-strain. This could be explained by the work hardening of the top sheet, which provides greater resistance to the rivet motion, thereby supporting the spread of the rivet foot. For the St-Al combination, the effect is observable, too. In the case of the St-St combination, the top sheets' increasing pre-strain shows a positive influence on the interlock development, while the opposite is true for the bottom sheet.

The influence of pre-strain on the bottom thickness shows similar trends for all combinations. For St-Al and St-St, increased pre-strains lead to smaller bottom thickness. This effect is more pronounced in the bottom sheet of the St-St combination than in the top sheet. This behaviour could be explained by the reduction in sheet thickness and its hardening. A strengthened sheet reduces the rivet foot's ability to spread, thereby increasing the distance from the foot's lowest tip to the bottom sheet end. The trend also appears to hold for the Al-Al combination, but further investigation with more data points at higher plastic strains is needed.

The pre-strain also influences the maximum shear-load capacity of the joints. Higher pre-strain reduces shear-load capacity. For the Al-Al combination, an increase in capacity is observed for strains up to 0.15–0.20 in the top sheet. The observed reduction below an EPS of 0.15 may be explained by increased sheet damage at higher strains, which outweighs the strengthening effects of work hardening. However, because damage is not calculated in this study, this remains a hypothesis until further research is conducted to verify it.

Summary

In this study, the influence of pre-strain on certain characteristics of self-piercing rivets is analysed. The study is carried out for three material-thickness combinations of the materials HCT590X and EN AW-6014 in the T4 condition. For all combinations, a numerical process chain was built in LS-DYNA to represent an application-oriented use case. The process chain comprised a simplified rolling process to introduce pre-strain, a 2D joining model of the SPR process, and a 3D model for shear tensile testing. A DoE was carried out for the entire process chain across all combinations, generating at least 100 data points. In detail, the influence of the pre-strain on characteristic geometrical values commonly used for SPR joint evaluation, as well as the load-bearing capacity of these joints, was investigated. The results show that the qualitative influence of pre-strain depends on the material combination. Currently, the material behavior is described without explicit damage modeling, leading to deviations between experiment and simulation particularly in the post-necking regime. Furthermore, friction was not modeled during the rolling process. To achieve accurate prediction of damage behavior, the model must be extended to incorporate friction effects.

Funding

The authors disclosed receipt of the following financial support for the research, authorship, and publication of this article: This research was supported by the Deutsche Forschungsgemeinschaft (DFG, German Research Foundation) – TRR 285/2 – 418701707. Data regarding the contents of the publication can be requested at www.trr285.de.

CRediT authorship contribution statement

J.-P. Ludwig: Writing – original draft, Software, Methodology, Investigation, Formal analysis, Data curation, Conceptualization. **E. Tolke:** Software, Methodology, Investigation, Formal analysis, Data curation. **M.C. Schlichter:** Visualization, Validation, Supervision, Resources, Formal analysis. **M. Bobbert:** Writing – review & editing, Supervision, Project administration, Methodology, Funding acquisition, Conceptualization. **G. Meschut:** Writing – review & editing, Supervision, Resources, Project administration, Funding acquisition.

Declaration of competing interest

The authors declare the following financial interests/personal relationships which may be considered as potential competing interests:

Jean-Patrick Ludwig reports financial support was provided by German Research Foundation. If there are other authors, they declare that they have no known competing financial interests or personal relationships that could have appeared to influence the work reported in this paper.

Acknowledgements

The authors thank the German Research Foundation for their organizational and financial support.

Data availability

Data will be made available on request.

References

Bielak, C., Böhnke, M., Beck, R., Bobbert, M., Meschut, G., 2021a. Numerical analysis of the robustness of clinching process considering the pre-forming of the parts. J. Adv. Join. Process. 3, 100038. https://doi.org/10.1016/j.jajp.2020.100038.

Bielak, C.R., Böhnke, M., Bobbert, M., Meschut, G., 2021b. Further development of a numerical method for analyzing the load capacity of clinched joints in versatile process chains. In: ESAFORM 2021. https://doi.org/10.25518/esaform21.4298.

Böhnke, M., Kappe, F., Bobbert, M., Meschut, G., 2021. Influence of various procedures for the determination of flow curves on the predictive accuracy of numerical simulations for mechanical joining processes. Mater. Test. 63 ((6), S), 493–500. https://doi.org/10.1515/mt-2020-0082.

Du, Z., Wei, B., He, Z., Cheng, A., Duan, L., Zhang, G., 2021. Experimental and numerical investigations of aluminium-steel self-piercing riveted joints under quasi-static and dynamic loadings. Thin Wall. Struct. 169, 108277.

Europäische Forschungsgesellschaft für Blechverarbeitung e.V, 2021. Merkblatt DVS/EFB 3480-1: Testing of Joint Properties. DVS Media GmbH, Düsseldorf in German.

S. Flachstahl. HCT590X+Z: dual-phase steel for cold forming. 2022. accessed on March 06, 2026 https://www.salzgitter-flachstahl.de/fileadmin/footage/MEDIA/gesellschaften/szfg/informationsmaterial/produktinformationen/feuerverzinkte_produkte/eng/hct600xd.pdf.

Friedlein, J., Bielak, C.R., Böhnke, M., Bobbert, M., Meschut, G., Mergheim, J., Steinmann, P., 2023. Influence of plastic orthotropy on clinching of sheet metal. Mater. Res. Proc. (25), 133–140. https://doi.org/10.21741/9781644902417-17.

Hahn, O., Kurzok, J.R., 1998a. Umformtechnisches Fügen Vorverformter Halbzeuge, 1. Shaker. Stahl.

Hahn, O., Kurzok, J.R., 1998b. Umformtechnisches Fügen Vorverformter Halbzeuge, 2. Shaker. Aluminium.

Han, L., Young, K.W., Chrysanthou, A., O'Sullivan, J.M., 2006. The effect of pre-straining on the mechanical behaviour of self-piercing riveted aluminium alloy sheets. Mater. Des. 27, 1108–1113.

Harabati, Ö., Bielak, C.R., Böhnke, M., Schlichter, M.C., Brockmeier, M., Bobbert, M., Meschut, G., 2025. Cross-process damage modeling: a process-chain case study of clinching and self-pierced riveting for aluminum connections. Mater. Res. Proc. 52, 150–158. https://doi.org/10.21741/9781644903551-19.

Holtkamp, P., Kappe, F., Probst, P., Bobbert, M., Meschut, G., 2025. Investigation of local heat treatment strategies for a multi-range capable rivet and the influence on joint formation and load-bearing capacity. Proc. Inst. Mech. Eng. L 239 (4), 787–800. https://doi.org/10.1177/14644207241307508.

Karathanasopoulos, N., Pandya, K.S., Mohr, D., 2021. An experimental and numerical investigation of the role of rivet and die design on the self-piercing riveting joint characteristics of aluminum and steel sheets. J. Manuf. Process. 69, 290–302.

Li, D., Han, L., Shergold, M., Thornton, M., Williams, G., 2013. Influence of rivet tip geometry on the joint quality and mechanical strengths of self-piercing riveted aluminium joints. LMT 765, 746.

Li, D., Chrysanthou, A., Patel, I., Williams, G., 2017. Self-piercing riveting-a review. Int. J. Adv. Manuf. Tech. 92 (5–8), 1777–1824.
Ma, Y., Lou, M., Li, Y., Lin, Z., 2018. Effect of rivet and die on self-piercing rivetability of AA6061-T6 and mild steel CR4 of different gauges. J. Mater. Process. Technol. 251, 282–294.
Meschut, G., Janzen, V., Olfermann, T., 2014. Innovative and highly productive joining technologies for multi-material lightweight car body structures. J. Mater. Eng. Perform. 23 (5), 1515–1523. https://doi.org/10.1007/s11665-014-0962-3.
Meschut, G., Merklein, M., Brosius, A., Drummer, D., Fratini, L., Füssel, U., Gude, M., Homberg, W., Martins, P.A.F., Bobbert, M., Lechner, M., Kupfer, R., Gröger, B., Han, D., Kalich, J., Kappe, F., Kleffel, T., Köhler, D., Kuball, C.-M., Popp, J., Römisch, D., Troschitz, J., Wischer, C., Wituschek, S., Wolf, M., 2022. Review on mechanical joining by plastic deformation. J. Adv. Join. Process. 5, 100113. https://doi.org/10.1016/j.jajp.2022.100113.
Neuser, M., Kappe, F., Busch, M., Grydin, O., Bobbert, M., Schaper, M., Meschut, G., Hausotte, T., 2021. Joining suitability of cast aluminium for self-piercing riveting. IOP Conf. Ser. 1157, 12005.
Novelis Global Automotive. EN AW-6014 T4 - material data sheet: novelis Advanz 6F - e170. 2019.
"Primer On Flat Rolling." Elsevier, 2014. doi: 10.1016/c2012-0-06474-5.
Schlichter, M.C., Harabati, Ö., Ludwig, J.-P., Böhnke, M., Bielak, C.R., Bobbert, M., Meschut, G., 2025. Experimental and numerical investigation of the influence of rolling-induced sheet metal deformation on SPR joints. Mater. Res. Proc. 54, 1364–1373. https://doi.org/10.21741/9781644903599-148.
Wang, D., Kong, D., Xie, C., Li, S., Zong, L., 2022. Study on the effect of rivet die parameters on joint quality of self-piercing riveting employed 3D modeling and MCDM method. Int. J. Adv. Manuf. Tech. 119 (11–12), 8227–8241.
Wang, C., Du, Z., Cheng, A., He, Z., Tan, H., Yu, W., 2023. Influence of process parameters and heat treatment on self-piercing riveting of high-strength steel and die-casting aluminium. J. Mater. Res. Technol. 26, 8857–8878.
Wang, C., Du, Z., Cheng, A., He, Z., 2024. Numerical investigation of joinability and forming quality improvement on self-piercing riveting process with varying sheet stack combinations. Thin Walled Struct. 201, 112017.
S. Werkstoff-Datenblatt, Saarstahl - 38B2, accessed on January 23, 2026 https://www.saarstahl.com/app/uploads/2024/03/20160226043414-38B2_deutsch.pdf.
Xie, Z., Yan, W., Yu, C., Mu, T., Song, L., 2018. Improved shear strength design of coldformed steel connection with single self-piercing rivet. Thin Wall. Struct. 131, 708–717.
Xue, Z., Wang, X., Xu, C., Chen, Z., Feng, X., Zhou, Q., et al., 2023. Equivalent characterization of prestrained material properties and mechanical behavior prediction of steel/aluminum self-piercing riveted joints. Thin-Walled Struct. 182, 110243.
Zhao, H., Han, L., Liu, Y.P., Liu, X.P., 2021. Quality prediction and rivet/die selection for SPR joints with artificial neural network and genetic algorithm. J. Manuf. Process. 66, 574–594.
Zhao, H., Han, L., Liu, Y., Liu, X., 2022. Analysis of joint formation mechanisms for selfpiercing riveting (SPR) process with varying joining parameters. J. Manuf. Process. 73, 668–685.